Scientia Iranica C (2019) 26(3), 1555–1565

SCIENTIA IRANICA

Sharif University of Technology
Scientia Iranica
Transactions C: Chemistry and Chemical Engineering
http://scientiairanica.sharif.edu

Research Note

Comparison of γ and δ-Al_2O_3 supported CoMo catalysts in the hydrodesulfurization of straight-run gas oil

M. Zarezadeh-Mehrizi, A. Afshar Ebrahimi*, and A. Rahimi

Iran Polymer and Petrochemical Institute, P.O. Box 14965/115, Tehran, Iran.

Received 9 June 2018; received in revised form 3 November 2018; accepted 4 February 2019

KEYWORDS
CoMo catalyst;
Alumina;
Hydrodesulfurization;
Boehmite;
Support structure.

Abstract. The effect of two different crystal species of alumina on the hydrodesulfurization activity of the corresponding CoMo catalysts was studied. Cylindrical extruded alumina with two different crystal structures, i.e., γ-Al_2O_3 and δ-Al_2O_3, was prepared using boehmite and nitric acid as a peptizing agent by calcination at 550°C and 900°C, respectively. Al_2O_3 supports were impregnated with 9 wt.% of Mo and 2 wt.% Co by an incipient wetness impregnation method. CoMo/Al_2O_3 catalysts were used for hydrodesulfurization (HDS) and hydrodenitrification (HDN) of Iranian Straight-Run Gas Oil (ISRGO). The supports and catalysts were characterized by nitrogen adsorption-desorption isotherm, XRD, UV-vis-DRS, TPD, TPR, CO chemisorption, and ICP-OES. The HDS activity of CoMo/γ-Al_2O_3 catalyst was higher than that of CoMo/δ-Al_2O_3 and was found to be 95.74%. This result was obtained from the formation of larger $CoMoO_4$ and MoO_3 crystals in CoMo/δ-Al_2O_3 catalyst, thus reducing the active metal phase dispersion and the performance of the catalyst. The HDS activity of CoMo/γ-Al_2O_3 catalyst was remarkable as the metal content of the catalyst was low. The HDN activity of CoMo/γ-Al_2O_3 was also about 66%.

1. Introduction

Hydrodesulfurization is a significant process in the refining industry. The quality of available crude oil has been decreasing year by year with a severe increase in sulfur and nitrogen contents [1-3]. Critical atmospheric pollution results from the presence of sulfur-containing compounds in transportation fuels. SO_x originates from the combustion of sulfur compounds, leading to the formation of acid rain [4]. Moreover, the exhaust emission treatment catalyst will be poisonous, and the corrosion of the internal combustion engines will be promoted in the presence of SO_x [5-7]. In addition, further conversion of heavy liquid hydrocarbons to more valuable products in terms of feasibility and economy depends on the quality and sulfur contents of the feedstock, indeed. On the other hand, environmental regulations necessitate limiting the amount of the sulfur component present in the fuel [8-13]. As a result, a decrease in sulfur content of refinery feedstock and fuel products is of environmental and industrial importance in the petroleum refining industry [14-18].

The conventional HDS catalysts can reduce a significant fraction of the high sulfur of raw middle distillate to 350-500 ppm. Ultra-low sulfur content can be achieved by an improved HDS catalyst or a two-stage process concept. The bulk of the sulfur content

*. *Corresponding author. Tel.: +98 21 48662484; Fax: +98 2144787032*
E-mail addresses: M. Zarezadeh-Mehrizi (M.Zarezadeh@ippi.ac.ir); A.Afshar@ippi.ac.ir (A. Afshar Ebrahimi); A.Rahimi@ippi.ac.ir (A. Rahimi).

doi: 10.24200/sci.2019.50969.1948

is removed in the first stage, and the HDS activity is about 91%. It is important to note that the metal content of these catalysts is about 25 wt.%, which is a high metal load. The hydrotreated product is then fed to the second reactor in order to perform ultra-deep desulfurization [19-20].

Alumina is the most common support used for hydrotreating catalyst because of its acceptable mechanical and intrinsic acid-base properties, low-cost prices, and tunable surface physicochemical properties [21-26]. The influence of the nature of the alumina support on the catalyst activity in HDS of straight-run gas oil was scarcely reported. Li et al. studied the activity of catalysts, prepared by incipient wetness impregnation of Co and Mo supported on two kinds of alumina in the HDS reaction of thiophene [27]. They found that lower interaction between the support and the active phase led to an increase in the activity. The comparison between three different alumina supports and various deposition methods with different Co precursors was reported by Laurenti et al. [28]. Different prepared catalytic systems were tested in HDS reactions of thiophene and 4,6-dimethylbenzothiophene. The results reflect that δ-alumina supported CoMoS catalyst was the most active CoMoS catalyst for the HDS of thiophene and 4,6-dimethylbenzothiophene. This was mainly attributed to better dispersion of the active phase on that support and lower interaction between the active component and the support surface.

In the present paper, the cylindrical extruded alumina support was calcined at two temperatures, i.e., 550°C and 900°C, in order to survey the effect of the nature of alumina support on metal-support interaction and acidity of the catalyst. The activity and performance of the catalysts were evaluated in the hydrodesulfurization of ISRGO. Nitrogen adsorption-desorption isotherm, XRD, UV-vis-DRS, TPD, and TPR were employed for the characterization of these catalysts.

2. Experimental

2.1. Materials

Ammonium heptamolybdate $(NH_4)_6Mo_7O_{24}.4H_2O$), cobalt acetate $(Co(CH_3COO)_2.4H_2O)$, citric acid $(C_6H_8O_7.H_2O)$, and nitric acid were used in the experiments. All materials were prepared by Merck Company and used without any purification. Boehmite (surface area: 275 m^2/g, pore volume: 0.71 cm^3/g, and pore diameter: 10.34 nm) was supplied by Iranian Institute of Research and Development in Chemical Industries.

2.2. Catalyst preparation

The extruded alumina support was prepared by the peptization of boehmite with nitric acid solution (3 wt%). The paste was kneaded and extruded. The resultant extruded alumina was dried at 110°C for 12 h. Then, calcination of the extruded alumina at 550°C for 4 h and at 900°C for 2 h in air resulted in γ-alumina and δ-alumina, respectively. The final support had a cylindrical form with an average diameter of 2.5 mm and a length of 4-6 mm. The bimetallic compound for catalyst preparation was synthesized via dissolution of citric acid of 0.234 mol and ammonium heptamolybdate of 0.328 mol in water. The solid cobalt acetate was added to this solution in proportion equivalent to the ratio of Mo/Co=2 atomic [29]. CoMo/γ-Al_2O_3 or CoMo/δ-Al_2O_3 catalysts with the same loading of 2 wt.% CoO and 9 wt.% MoO_3 were prepared by the incipient wetness impregnation of extruded alumina with a rose-colored clear aqueous solution of bimetallic complex. The wet impregnated extruded catalyst was dried at room temperature and, then, at 110°C for 12 h. Mo and Co contents of catalysts were kept constant at 9 wt.% of MoO_3 and 2 wt.% of CoO.

2.3. Catalytic activity test for ISRGO hydrodesulforization

The HDS activity tests were carried out in a continuous trickle-bed reactor. Straight-run gas oil with the total sulfur content of 0.94 wt% was used as the feedstock. The feedstock properties are shown in Table 1. In a typical run, 7 ml of the catalyst was loaded into the reactor. Silicon carbide was also loaded into both ends of the reactor as inert support of the catalyst bed. The schematic of the activation process is presented in Figure 1.

Each hydrodesulfurization experiment was performed for 3 days at 7 MPa, T = 370°C, LHSV = 2 h^{-1}, and H_2/feed volume ratio of 174.

The total sulfur content of hydrodesulfurized product oil samples was analyzed by X-Ray Fluorescence spectrometry (XRF).

The % HDS activity of the catalysts was obtained by the following formula:

$$\text{HDS activity (\%)} = \text{[1-sulfur content of product/sulfur content of feed]} \times 100. \quad (1)$$

2.4. Catalyst characterization

2.4.1. Elemental analysis

The elemental composition of the catalysts was determined by the inductively coupled plasma optical emis-

Table 1. Properties of feedstock (ISRGO).

Density (g/cm^3) at 15°C	0.86
Sulfur content (mass %)	0.94
Nitrogen content (mass %)	0.03
Initial boiling point (°C)	171.4
Final boiling point (°C)	371.7

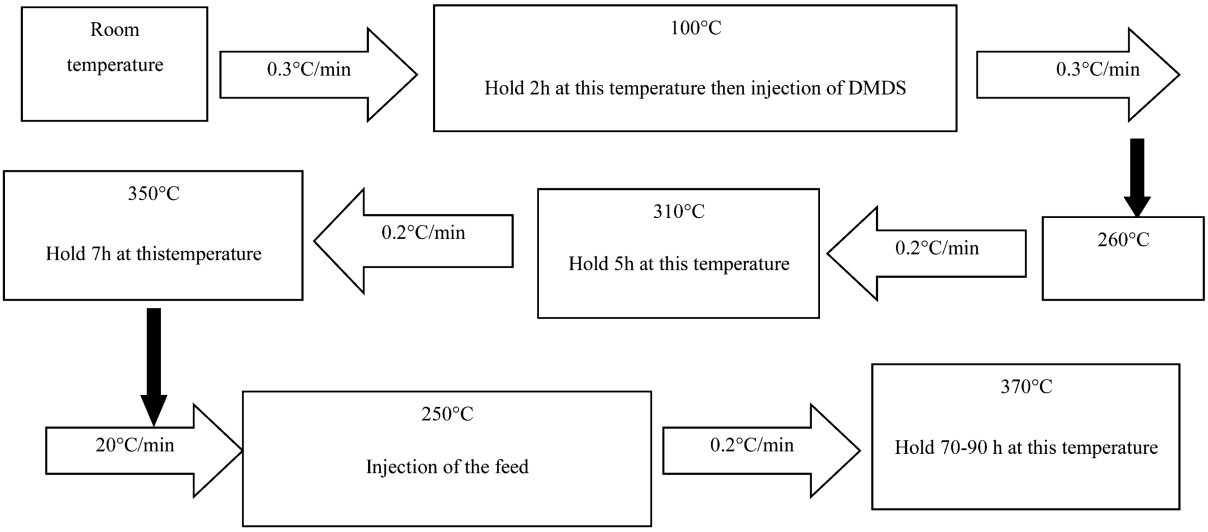

Figure 1. Schematic of activation process of HDS catalyst.

sion spectroscopy (ICP-OES) Varian 730-ES (America).

2.4.2. Textural properties

The specific surface area, pore volume, and pore size distribution of extruded alumina before and after impregnation were obtained from nitrogen adsorption-desorption isotherms, determined at −196°C with Belsorp min II apparatus. The alumina and impregnated alumina were degassed at 300°C and 150°C for 5 h, respectively. The specific surface area of the samples was calculated according to Brunauer-Emmett-Teller (BET) method, and the pore size distribution and total pore volume were determined from the adsorption branches of the corresponding nitrogen isotherm by the Barrett-Joyner-Halenda (BJH) method.

2.4.3. Crushing strength

The crushing strength of the extruded alumina was determined by measuring the breaking force for a sample compressed between two parallel plates using a Santam STM-20 (Iranian) machine according to ASTM D 6175. The Side Crushing Strength (SCS) was calculated through the following equation:

$$SCS = F/L, \tag{2}$$

where F is Force (N), and L is the length of the extruded catalyst (mm). In the Lateral Crushing Strength (LCS) measurements, the cross-sectional area of the granule was taken to be $S = DL$, where D is the granule diameter (cm) and L is the granular length (cm):

$$LCS = F/S. \tag{3}$$

2.4.4. Ultraviolet visible diffuse reflectance spectroscopy (UV-vis DRS)

UV-vis DRS spectra were collected in air on an Avaspec-2048-TEC in the wavelength range of 200-1100 nm using $BaSO_4$ powder as a reference.

2.4.5. X-ray diffraction

X-Ray powder Diffraction (XRD) patterns were taken at room temperature on a SIEMENS D-5000 in the range angle from 5 to 70 degree using Cu Kα radiation.

2.4.6. Temperature-programmed desorption of ammonia (NH_3-TPD)

The acidity of the oxide catalysts was analyzed by Temperature-Programmed Desorption (TPD) of ammonia with a Micrometrics 2900 apparatus provided with a Thermal Conductivity Detector (TCD) and interfaced to a data station. A sample of 20 mg was outgassed in a He flow at 573 K for 1.5 h. In the next step, the catalyst was saturated with ammonia at 353 K for 30 min. After equilibrium, ammonia desorption was done by heating the catalysts at a linear temperature ramp of 10°C /min from 25°C up to 750°C.

2.4.7. Temperature-programmed reduction (H_2-TPR)

The reduction behavior of the oxide catalysts was studied by TPR on a Micrometrics 2900 apparatus provided with a TCD and interfaced to a data station. In this respect, 50 mg of the calcined catalyst was heated at a linear temperature ramp of 10°C /min from 25°C to 300°C and kept for 90 min under a He flow to remove water and other contaminations. The catalysts were cooled to ambient temperature in the same He flow. The reduction was carried out in a 5% H_2 in argon and heated at a rate of 10°C/min to the final temperature of 750°C.

2.4.8. CO chemisorptions

Pulse CO chemisorption was measured with NanoSORD NS91 (Sensiran, Iran). A sample was

pretreated under H_2 flow at 350°C in the presence of H_2 for 6 h. The sample was cooled down to 35°C; then, CO chemisorption analysis was performed by introducing a successive pulse of 10% CO in He.

3. Results and discussion

Cobalt and molybdenum contents of the calcined catalysts, determined by the inductively coupled plasma optical emission spectroscopy, are given in Table 2.

The textural properties, such as specific surface area, pore size distribution, pore volume of the supports, and corresponding CoMo catalysts, were evaluated by nitrogen adsorption-desorption isotherms, and these physical characteristics are presented in Table 3. The N_2 adsorption-desorption isotherm of the γ-alumina support and its catalyst are attributed to IV type (Figure 2). The nitrogen isotherm of the samples reveals a hysteresis loop of H1-type, confirming the presence of cylindrical pores in the support and catalysts [30]. The form of pores for the support and catalyst is similar, because the hysteresis loop does not change after impregnation.

The effect of metal impregnation on the textural properties of γ-Al_2O_3 can be obtained by comparing their N_2 adsorption-desorption isotherms with that of pure support. In Figure 2, a decrease in the amount of adsorbed nitrogen is observed after the impregnation of Co and Mo on the support, resulting from the metal oxides species formed within the inner porous structure and on the support surface. The preservation of hysteresis loop shape for CoMo/γ-Al_2O_3 catalyst confirms that there is no plugging of mesopores and, also, no changes in the support structure after impregnation.

N_2 adsorption-desorption isotherms of δ-Al_2O_3 and CoMo/δ-Al_2O_3 are presented in Figure 3 that exhibit the characteristics of type-IV isotherm. The hysteresis loop of γ-Al_2O_3 shifts from the uptake of nitrogen at a relative pressure P/P0 of 0.5 to 0.7 in δ-Al_2O_3, indicating the presence of larger pore diameters in δ-Al_2O_3. The amount of adsorbed nitrogen is increased upon incorporation of metal into δ-Al_2O_3, implying that the impregnation of δ-Al_2O_3 increases the specific surface area and pore volume significantly (Table 3). This phenomenon may result from the

Table 2. Composition of fresh catalyst oxide.

Catalyst	Composition (wt.%)[a]	
	CoO	MoO_3
CoMo/γ-Al_2O_3	2	9
CoMo/δ-Al_2O_3	2	9

[a] These nominal values have been confirmed by ICP-OES and found to be in close agreement.

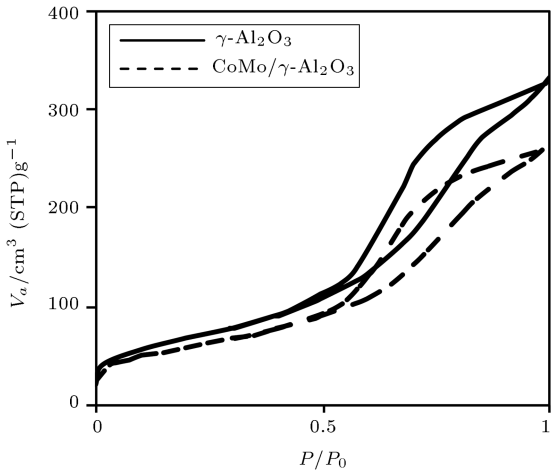

Figure 2. N_2 adsorption-desorption isotherms of γ-Al_2O_3 and CoMo/γ-Al_2O_3 catalysts.

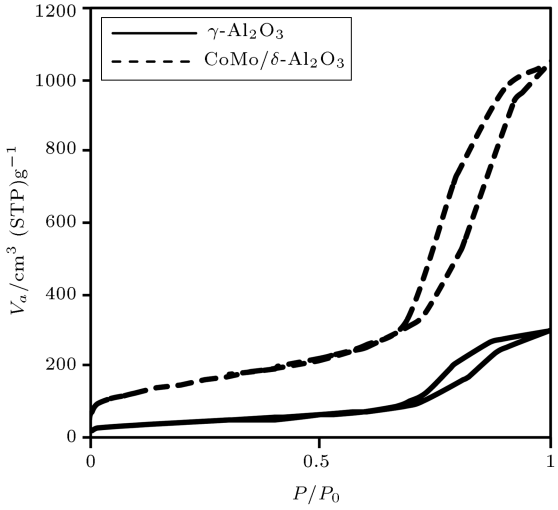

Figure 3. N_2 adsorption-desorption isotherms of δ-Al_2O_3 and CoMo/δ-Al_2O_3 catalysts.

Table 3. Textural properties of supports and fresh catalysts.

Sample	BET surface area (m^2/g)	Total pore volume (cm^3/g)	Average pore diameter (nm)	BJH pore diameter (nm)
γ-Al_2O_3	240.49	0.5062	8.94	5.42
CoMo/γ-Al_2O_3	204.24	0.4059	7.94	6.18
δ-Al_2O_3	153	0.46	12	8
CoMo/δ-Al_2O_3	556	1.6	11.5	8

formation of metal oxides particles in the pores that led to an increase in surface area and pore volume.

The addition of Co and Mo to γ-Al_2O_3 leads to a decrease in surface area and pore volume. The pore size calculated by BJH method reflects an increase in the pore diameter. Impregnation may initially block small pores and produce an increase in an apparent average size of unblocked pores. This phenomenon shows a decrease in average pore size with impregnation, as presented in Table 3. On the other hand, CoMo/δ -Al_2O_3 demonstrates significant textural changes during the catalyst preparation. A 3.6-fold increase in specific surface area is observed, which can be explained by the contribution of the active phase to the total specific surface area.

The pore volume in different pores is presented in Table 4. The pore volumes of γ-Al_2O_3 and δ-Al_2O_3 derived from pores larger than 10 nm were about 36% and 64 %, respectively. These results showed that calcination at high temperatures increased the pore size of alumina. The volume of pores between 10-20 nm in δ-Al_2O_3 is seven times greater than that of γ-Al_2O_3. The pore volume of all pore ranges increases after impregnation of δ-Al_2O_3, which indicates the formation of a new porosity phase.

Figure 4 shows the pore size distribution of alumina supports and catalysts. It is observed that the pore size distribution of δ-Al_2O_3 is tri-modal at 5, 8, and 12 nm; however, γ-Al_2O_3 shows bi-modal behavior at 5 and 8 nm. Calcination at 900°C increased the pore diameter of the support. The impregnation of γ-Al_2O_3 reduced the intensity of the pore size distribution curves due to a decrease in the number of pores less than 5 nm in diameters (Figure 4(a)). The intensity of pore size distribution of CoMo/δ-Al_2O_3 is higher than that of δ-Al_2O_3, indicating an increase in the surface area and pore volume after impregnation, as summarized in Table 3. The main reason for this phenomenon is not obvious; however, it is assumed that the metal component increases surface roughness and forms particles of metal oxides in larger pores without plugging and introducing new pores. Lower activity of CoMo/δ-Al_2O_3 catalyst may be due to the enhanced formation of large $CoMoO_4$ crystals, as noticed from XRD, causing loss of Mo dispersion and, on the other hand, requiring higher temperature for sulfiding.

The side and lateral crushing strengths of the extruded γ-Al_2O_3 were 9.3 N/mm and 435 N/cm^2, respectively, which is much higher than 329 N/cm^2 of the sample reported by Parkhomchuk et al. [31], 360 N/cm^2 reported by Laurer [32], and 97 N/cm^2 reported by Wassermann and Meyer [33]. This difference is possibly due to various preparation details and characteristics of starting materials.

The diffuse UV-visible reflectance spectra of catalysts are depicted in Figure 5. The intense adsorption band at about 200-400 nm could be commonly assigned to the Charge Transfer (CT) transitions, i.e., oxygen

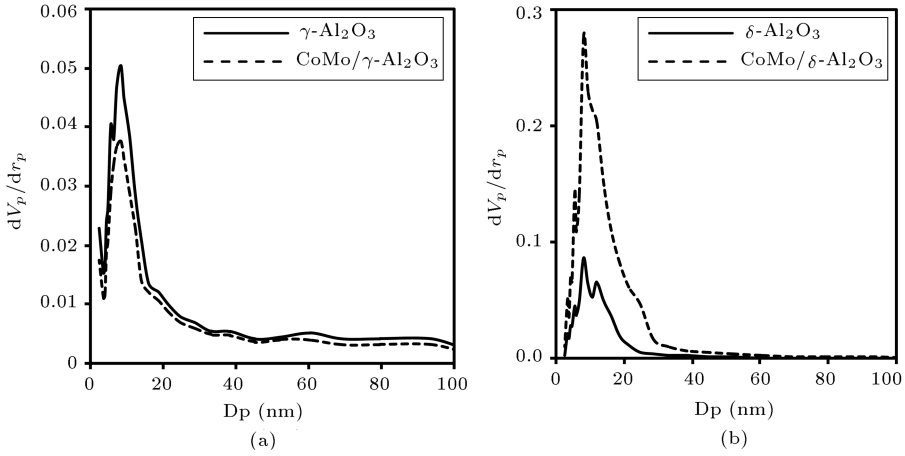

Figure 4. Pore size distribution of alumina supports and catalysts.

Table 4. Distribution of pore volume in different pore diameters.

Sample	Pore volume distribution in different pore diameters (ml/g)						Total pore volume (ml/g)
	0-3 nm	3-5 nm	5-10 nm	10-20 nm	20-30 nm	+30 nm	
γ-Al_2O_3	0.0229	0.0819	0.2204	0.1135	0.0246	0.0476	0.5109
CoMo/γ-Al_2O_3	0.0176	0.062	0.1715	0.0881	0.0217	0.03873	0.3996
$\delta-Al_2O_3$	0.0018	0.0243	0.14	0.2094	0.0369	0.047	0.4595
CoMo/δ-Al_2O_3	0.0068	0.0571	0.4523	0.7092	0.2101	0.1429	1.5784

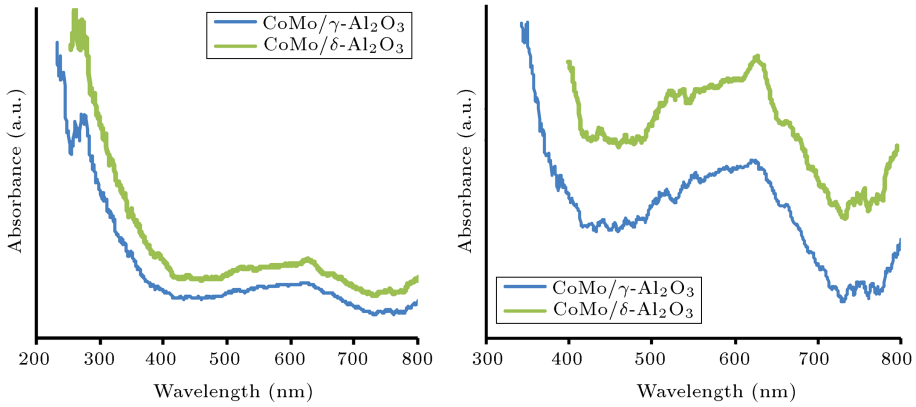

Figure 5. DRS UV-vis of CoMo/γ-Al_2O_3 and CoMo/δ-Al_2O_3.

ligand to molybdenium ions (Mo^{6+}) of both tetrahedral and octahedral species [34-36]. In addition to Mo^{6+} CT that appeared in the UV region, the visible spectra of the catalysts exhibited band in the range of 450-700 nm associated with Co species. Both CoMo/γ-Al_2O_3 and CoMo/δ-Al_2O_3 showed a triplet broadband in the range of 450-750 nm (545, 580-595, and 630 nm), which can be attributed to d-d transitions of inactivate tetrahedral cobalt (II) ions in $CoAlO_4$. The intensity of the peak at 630 in CoMo/γ-Al_2O_3 was lower than that of CoMo/δ-Al_2O_3, indicating an increase in the amount of catalytically active cobalt species in CoMo/γ-Al_2O_3 catalyst. The maximum peak at 750 nm is ascribed to octahedral Co^{2+} species, which was in both forms of the catalysts [37]. CoMo/δ-Al_2O_3 exhibited a band at 520 nm and a shoulder at 680 nm. The band at 520 nm belongs to the characteristic peak of d-d transition of high spin octahedral Co^{2+} complexes in β-$CoMoO_4$. The shoulder at 680 nm can be attributed to d-d transitions of Co^{2+} ions in tetrahedral coordination in Co_3O_4 [38].

Figure 6 shows the wide-angle X-ray diffraction of γ-Al_2O_3 and CoMo/γ-Al_2O_3. The XRD pattern of the support is similar to γ phase. No obvious peaks in the crystalline form of $CoMoO_4$ were observed in the XRD pattern of CoMo/γ-Al_2O_3, indicating that Co and Mo species were highly dispersed over γ-Al_2O_3 [5].

The diffraction peaks of δ-Al_2O_3 (Figure 7) are more intense and narrower than those of γ-Al_2O_3, demonstrating better crystallinity. The observed patterns could be attributed to the presence of δ-phase due to the separation of reflexes 220 and 400 [31]. Following the loading of cobalt and molybdenum, the peaks at 23.4, 26.2, and 27.4° are observed in the XRD pattern. The diffraction peaks at 23.4 and 26.2 are assigned to the crystalline $CoMoO_4$ phase. The peak at 2θ=27.4 can be attributed to the presence of MoO_3 phase [37,39-40]. It can be concluded that the catalyst supported on γ-Al_2O_3 had a higher dispersion of $CoMoO_4$ phase than that of δ-Al_2O_3, thus preventing the formation of large crystalline MoO_3 and $CoMoO_4$ phases. The absence of any metal oxide diffraction peak ensured that CoMo/γ-Al_2O_3 catalyst tended to contain small metal particles of crystal sizes below the detection limit of the XRD. The XRD results are in good agreement with the DRS results.

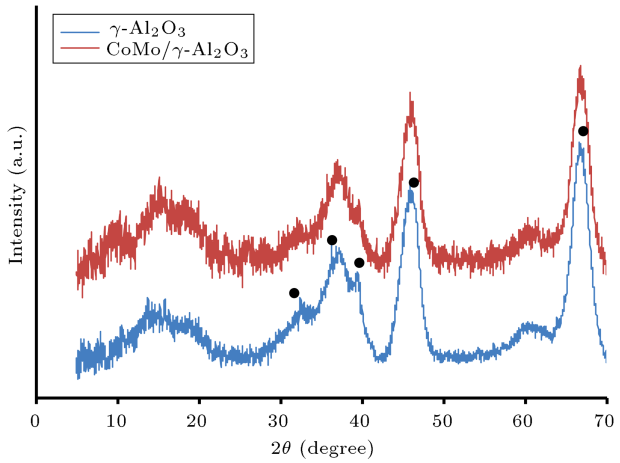

Figure 6. X-ray diffraction patterns of γ-Al_2O_3 and CoMo/γ-Al_2O_3.

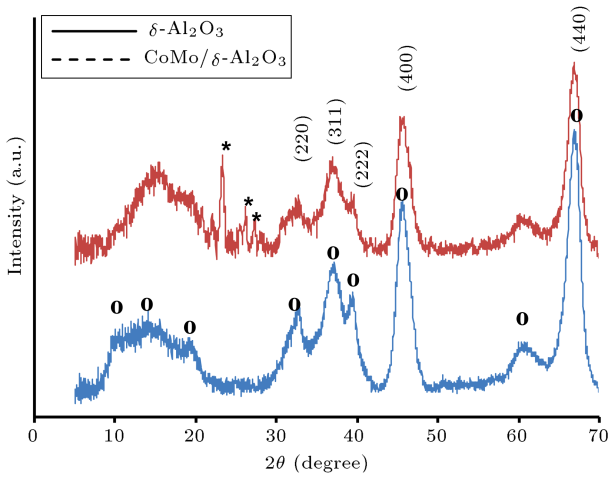

Figure 7. X-ray diffraction patterns of δ-Al_2O_3 and CoMo/δ-Al_2O_3.

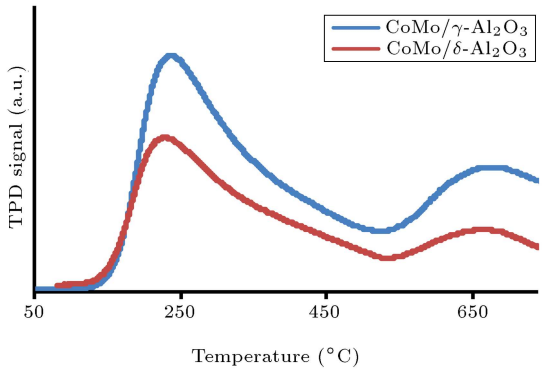

Figure 8. TPD-NH_3 profiles of the calcined catalysts.

The TPD of ammonia profiles provides necessary information about the acidity of the catalysts. The low desorption temperature peak is attributed to the desorption of ammonia over weak acidic sites, and the high desorption temperature peak corresponds to the desorption of ammonia from strong acid sites [41]. NH_3-TPD profiles of catalysts are presented in Figure 8. The total acidity and the acid sites distribution of calcined samples, expressed as mmol of desorption NH_3 per g of catalyst, are reported in Table 5.

In Table 5, the weak, strong, and total acid sites follow the trend: $CoMo/\gamma\text{-}Al_2O_3$>$CoMo/\delta\text{-}Al_2O_3$. The strong acid sites have been significantly dropped by increasing the calcination temperature of the support, which is in good agreement with literature results [42-44]. This correlates with the ratios of the support surface area and their dehydroxylation during the calcination.

The metal-support interaction and redox behavior of the oxide catalysts can be obtained by TPR techniques. The TPR profiles of the calcined catalysts are displayed in Figure 9. The $CoMo/\gamma\text{-}Al_2O_3$ catalyst showed the reduction peak at around 539°C, which was due to a reduction in $CoMoO_4$ [37,40,45-46]. This

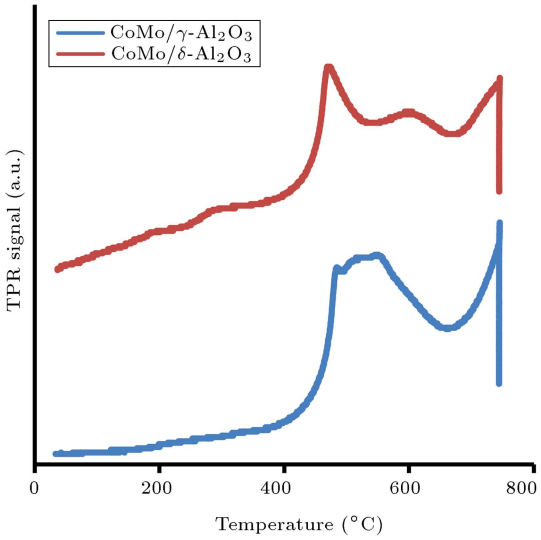

Figure 9. TPR profiles of the oxide catalysts.

peak shifted to higher temperatures around 570°C for $CoMo/\delta\text{-}Al_2O_3$, indicating that the metal-support interaction increased and the dispersity of Mo and Co oxide species reduced [5,47]. The higher dispersion of metal component promoted the reduction of Mo species, thus decreasing the reduction temperature in $CoMo/\gamma\text{-}Al_2O_3$. The H_2 uptake values were calculated (Table 6) in order to evaluate the corresponding hydrogen consumption. The $CoMo/\delta\text{-}Al_2O_3$ catalyst consumed 1.5-fold H_2 regarding $CoMo/\gamma\text{-}Al_2O_3$, which indicated the larger amount of $CoMoO_4$ phase formation on the surface of $\delta\text{-}Al_2O_3$. The wide peak from 500 to 700°C can be attributed to the first step of MoO_3 reduction to MoO_2 (Mo^{6+} to Mo^{4+}), whereas the hydrogen consumption at temperatures above 700°C can be ascribed to the reduction of MoO_2 to MoO [48-49]. The peak at about 460°C for $CoMo/\delta\text{-}Al_2O_3$ has been attributed to the bulk cobalt oxide reduction, while the absence of that in $CoMo/\gamma\text{-}Al_2O_3$ demonstrated better dispersion of Co and Mo species [5].

Table 5. Acidity of the CoMo oxide catalysts as determined by NH_3-TPD.

Catalyst	Strength of acid sites (mmol NH_3/g_{cat})		
	Weak (T < 300)	Strong (T > 500°C)	Total
$CoMo/\gamma\text{-}Al_2O_3$	0.8046	0.7088	1.5134
$CoMo/\delta\text{-}Al_2O_3$	0.6390	0.2464	0.8854

Table 6. H_2 uptake (from TPR) for calcined catalysts.

Catalyst	H_2 uptake (mmol/g_{cat})		
	First peak	Second peak	Total
$CoMo/\gamma\text{-}Al_2O_3$	0.3797	0.6049	0.9846
$CoMo/\delta\text{-}Al_2O_3$	0.6229	0.6420	1.2649

Table 7. CO uptake parameters of CoMo-alumina catalysts.

Sample	Metal dispersion (%)	Metallic surface area (m^2/g of metal)	Crystallite size (nm)	CO adsorbed (μmol/g)
CoMo/γ-Al_2O_3	15	74	9	38
CoMo/δ-Al_2O_3	11	55	12	28

Table 8. Sulfur and nitrogen content of feedstock and product and HDS and HDN activity of catalysts in hydrotreating tests.

Sample	Sulfur content (ppm)	HDS% activity	Nitrogen content (ppm)	HDN% activity
Feedstock	9400	–	300	–
Product of CoMo/γ-Al_2O_3	400	95.74	100	66.67
Product of CoMo/δ-Al_2O_3	3098	67.04	200	33.33

The CO chemisorption values of the oxide catalysts are included in Table 7. It can be seen that the metal dispersion and quantity of CO adsorbed of CoMo/γ-Al_2O_3 are higher than those of CoMo/δ-Al_2O_3.

The test results of the prepared catalysts in HDS and HDN of ISRGO are presented in Table 8. The HDS and HDN activity of CoMo/γ-Al_2O_3 is much higher than that of CoMo/δ-Al_2O_3. The higher activity of CoMo/γ-Al_2O_3 can be attributed to the lack of the formation of large crystalline $CoMoO_4$ phase in CoMo/γ-Al_2O_3 catalyst according to the XRD patterns of catalysts and better dispersion of Co and Mo. This is confirmed by CO chemisorptions analysis results. It has been reported that catalysts containing $CoMoO_4$ are more difficult to sulfide and exhibit lower HDS activity [39]. On the other hand, Co and Mo species were mainly dispersed on the surface of the smaller mesopores, while the smaller mesopores were reduced in the prepared δ-Al_2O_3 based on N_2 adsorption-desorption isotherms. In the δ-Al_2O_3 support, the increase of large mesopores and macropores enhanced the diffusion rate of feedstock molecules into these pores so that the HDS activity of the catalyst fell down significantly in comparison with γ-Al_2O_3. It is possible that although the activity of δ-Al_2O_3 supported sulfide catalyst is higher than that of the γ-Al_2O_3 supported catalyst in the HDS of model sulfur containing compounds, they are not good candidates for HDS of the real gas oil fraction.

4. Conclusion

The cylindrical γ-Al_2O_3 and δ-Al_2O_3 supports with surface areas of 240 and 153 m^2/g, pore volumes of 0.5 and 0.46 cm^3/g, and average pore diameters of 8.94 and 12 nm were prepared by extrusion of peptized boehmite paste calcined at 550 and 900°C, respectively. The preparation of CoMo/alumina catalysts was carried out by the incipient wetness impregnation method with a clear purple aqueous solution of bimetallic complex compound prepared by ammonium heptamolybdate, cobalt acetate, and citric acid as a chelating agent. The catalyst contains 2 wt% Co and 9 wt% Mo. The prepared CoMo/alumina catalyst was used for the hydrodesulfurization and hydrodenitrification (HDN) of ISRGO. It was found that CoMo/γ-Al_2O_3 and CoMo/δ-Al_2O_3 catalysts could reduce sulfur content of ISRGO from 9400 ppm (0.94 wt%) to 400 ppm (0.04 wt%) and 3098 ppm (0.3098 wt%) in the product, respectively. Lower activity of CoMo/δ-Al_2O_3 catalyst may result from the enhanced formation of large $CoMoO_4$ crystals, as noticed from XRD, causing loss of Mo dispersion and, on the other hand, requiring higher temperatures for sulfiding confirmed by CO chemisorptions' results. The produced catalyst with a low metal content of about 11 wt.% may be a good candidate for the bulk sulfur reduction in the first stage of the HDS process with HDS activity of about 96% for ISRGO, and the remaining sulfur content can be removed in the second stage.

Acknowledgment

The authors are grateful to financial support from Iran National Science Foundation (Grant No.94028719) and Iran polymer and petrochemical institute (Project No. 24754103).

References

1. Badoga, S., Mouli, K.C., Soni, K.K., Dalai, A.K., and Adjaye, J. "Beneficial influence of EDTA on the structure and catalytic properties of sulfided NiMo/SBA-15 catalysts for hydrotreating of light gas oil", *Applied Catalysis B: Environmental*, **125**, pp. 67-84 (2012).
2. Tao, X., Zhou, Y., Wei, Q., Ding, S., Zhou, W., Liu, T.,

and Li, X. "Inhibiting effects of nitrogen compounds on deep hydrodesulfurization of straight-run gas oil over a NiW/Al_2O_3 catalyst", *Fuel*, **188**, pp. 401-407 (2017).

3. Usman Kubota, T., Hiromitsu, I., and Okamoto, Y. "Effect of boron addition on the surface structure of Co-Mo/Al_2O_3 catalysts", *Journal of Catalysis*, **247**(1), pp. 78-85 (2007).

4. Al-Hammadi, S.A., Al-Amer, A.M., and Saleh, T.A. "Alumina-carbon nanofiber composite as a support for MoCo catalysts in hydrodesulfurization reactions", *Chemical Engineering Journal*, **345**, pp. 242-251 (2018).

5. Liu, X., Li, X., and Yan, Z. "Facile route to prepare bimodal mesoporous γ-Al_2O_3 as support for highly active CoMo-based hydrodesulfurization catalyst", *Applied Catalysis B: Environmental*, **121-122**, pp. 50-56 (2012).

6. De Souza, W.F., Guimarães, I.R., Guerreiro, M.C., and Oliveira, L.C.A. "Catalytic oxidation of sulfur and nitrogen compounds from diesel fuel", *Applied Catalysis A: General*, **360**(2), pp. 205-209 (2009).

7. Rezaee, M., Kazemeini, M., Fattahi, M., Rashidi, A.M., and Vafajoo, L. "Oxidation of H_2S to elemental sulfur over alumina based nanocatalysts: Synthesis and physiochemical evaluations", *Scientia Iranica*, **23**(3), pp. 1160-1174 (2016).

8. El Sayed, H.A., El Naggar, A.M.A., Heakal, B.H., Ahmed, N.E., Said, S., and Abdel-Rahman, A.A.H. "Deep catalytic desulphurization of heavy gas oil at mild operating conditions using self-functionalized nanoparticles as a novel catalyst", *Fuel*, **209**, pp. 127-131 (2017).

9. Van Haandel, L., Hensen, E.J.M., and Weber, T. "High pressure flow reactor for in situ X-ray absorption spectroscopy of catalysts in gas-liquid mixtures - A case study on gas and liquid phase activation of a CoMo/Al2O3 hydrodesulfurization catalyst", *Catalysis Today*, **292**, pp. 51-57 (2017).

10. Badoga, S., Ganesan, A., Dalai, A.K., and Chand, S. "Effect of synthesis technique on the activity of CoNiMo tri-metallic catalyst for hydrotreating of heavy gas oil", *Catalysis Today*, **291**, pp. 160-171 (2017).

11. Van Haandel, L., Bremmer, G.M., Hensen, E.J.M., and Weber, T. "Influence of sulfiding agent and pressure on structure and performance of CoMo/Al2O3 hydrodesulfurization catalysts", *Journal of Catalysis*, **342**, pp. 27-39 (2016).

12. Jaf, Z.N., Altarawneh, M., Miran, H.A., Jiang, Z.-T., and Dlugogorski, B.Z. "Hydrodesulfurization of thiophene over γ-Mo2N catalyst", *Molecular Catalysis*, **459**, pp. 21-30 (2018).

13. Huang, T., Xu, J., and Fan, Y. "Effects of concentration and microstructure of active phases on the selective hydrodesulfurization performance of sulfided CoMo/Al2O3 catalysts", *Applied Catalysis B: Environmental*, **220**, pp. 42-56 (2018).

14. Miño, A., Lancelot, C., Blanchard, P., Lamonier, C., Rouleau, L., Roy-Auberger, M., Royer, S., and Payen, E. "Strategy to produce highly loaded alumina supported CoMo-S catalyst for straight run gas oil hydrodesulfurization", *Applied Catalysis A: General*, **530**, pp. 145-153 (2017).

15. Dorneles de Mello, M., de Almeida Braggio, F., da Costa Magalhães, B., Zotin, J.L., and da Silva, M.A.P. "Kinetic modeling of deep hydrodesulfurization of dibenzothiophenes on NiMo/alumina catalysts modified by phosphorus", *Fuel Processing Technology*, **177**, pp. 66-74 (2018).

16. Saleh, T.A., Al-Hammadi, S.A., Abdullahi, I.M., and Mustaqeem, M. "Synthesis of molybdenum cobalt nanocatalysts supported on carbon for hydrodesulfurization of liquid fuels", *Journal of Molecular Liquids*, **272**, pp. 715-721 (2018).

17. Dong, Y., Xu, Y., Zhang, Y., Lian, X., Yi, X., Zhou, Y., and Fang, W. "Synthesis of hierarchically structured alumina support with adjustable nanocrystalline aggregation towards efficient hydrodesulfurization", *Applied Catalysis A: General*, **559**, pp. 30-39 (2018).

18. Han, W., Nie, H., Long, X., Li, M., Yang, Q., and Li, D. "Effects of the support Brønsted acidity on the hydrodesulfurization and hydrodenitrogention activity of sulfided NiMo/Al2O3 catalysts", *Catalysis Today*, **292**, pp. 58-66 (2017).

19. Ho, T.C. and Markley, G.E. "Property-reactivity correlation for hydrodesulfurization of prehydrotreated distillates", *Applied Catalysis A: General*, **267**(1-2), pp. 245-250 (2004).

20. Pang, W.W., Zhang, Y.Z., Choi, K.H., Lee, J.K., Yoon, S.H., Mochida, I., and Nakano, K. "Design of catalyst support for deep hydrodesulfurization of gas oil", *Petroleum Science and Technology*, **27**(12), pp. 1349-1359 (2009).

21. Asadi, A.A., Alavi, S.M., Royaee, S.J., and Bazmi, M. "Ultradeep hydrodesulfurization of feedstock containing cracked gasoil through NiMo/γ-Al2O3 catalyst pore size optimization", *Energy & fuels*, **32**(2), pp. 2203-2212 (2018).

22. Vozka, P., Orazgaliyeva, D., Šimáček, P., Blažek, J., and Kilaz, G. "Activity comparison of Ni-Mo/Al2O3 and Ni-Mo/TiO2 catalysts in hydroprocessing of middle petroleum distillates and their blend with rapeseed oil", *Fuel Processing Technology*, **167**, pp. 684-694 (2017).

23. Badoga, S., Sharma, R.V., Dalai, A.K., and Adjaye, J. "Synthesis and characterization of mesoporous aluminas with different pore sizes: Application in NiMo supported catalyst for hydrotreating of heavy gas oil", *Applied Catalysis A: General*, **489**, pp. 86-97 (2015).

24. Badoga, S., Dalai, A.K., Adjaye, J., and Hu, Y. "Insights into individual and combined effects of phosphorus and EDTA on performance of NiMo/MesoAl_2O_3 catalyst for hydrotreating of heavy gas oil", *Fuel Processing Technology*, **159** pp. 232-246 (2017).

25. Liu, D., Wang, A., Liu, C., and Prins, R. "Ni2P/Al2O3 hydrodesulfurization catalysts prepared by separating the nickel compound and hypophosphite", *Catalysis Today*, **292**, pp. 133-142 (2017).

26. Zarezadeh-Mehrizi, M., Afshar Ebrahimi, A., and Rahimi, A. "Preparation of extruded alumina with suitable crushing strength and good stability", *Scientia Iranica*, **25**(3), pp. 1434-1439 (2018).

27. Li, M., Li, H., Jiang, F., Chu, Y., and Nie, H. "Effect of surface characteristics of different alumina on metal-support interaction and hydrodesulfurization activity", *Fuel*, **88**(7), pp. 1281-1285 (2009).

28. Laurenti, D., Phung-Ngoc, B., Roukoss, C., Devers, E., Marchand, K., Massin, L., Lemaitre, L., Legens, C., Quoineaud, A.-A., and Vrinat, M. "Intrinsic potential of alumina-supported CoMo catalysts in HDS: Comparison between γc, γT, and δ-alumina", *Journal of Catalysis*, **297**, pp. 165-175 (2013).

29. Pashigreva, A.V., Bukhtiyarova, G.A., Klimov, O.V., Chesalov, Y.A., Litvak, G.S., and Noskov, A.S. "Activity and sulfidation behavior of the CoMo/Al2O3 hydrotreating catalyst: The effect of drying conditions", *Catalysis Today*, **149**(1-2), pp. 19-27 (2010).

30. Thommes, M., Kaneko, K., Neimark, A.V., Olivier, J.P., Rodriguez-Reinoso, F., Rouquerol, J., and Sing, K.S. "Physisorption of gases, with special reference to the evaluation of surface area and pore size distribution (IUPAC technical report)", *Pure and Applied Chemistry*, **87**(9-10), pp. 1051-1069 (2015).

31. Parkhomchuk, E.V., Lysikov, A.I., Okunev, A.G., Parunin, P.D., Semeikina, V.S., Ayupov, A.B., Trunova, V.A., and Parmon, V.N. "Meso/ Macroporous CoMo alumina pellets for hydrotreating of heavy oil", *Industrial & Engineering Chemistry Research*, **52**(48), pp. 17117-17125 (2013).

32. Laurer, P.R., *Preparation of a Catalyst Carrier from Alumina Mixtures*, Google Patents (1981).

33. Wassermann, M. and Meyer, A., *Process for Making Extrudates from Aluminum Oxyhydrates*, Google Patents (1977).

34. Ramírez, J., Castillo, P., Cedenõ, L., Cuevas, R., Castillo, M., Palacios, J., and López-Agudo, A. "Effect of boron addition on the activity and selectivity of hydrotreating CoMo/Al2O3 catalysts", *Applied Catalysis A: General*, **132**(2), pp. 317-334 (1995).

35. Nicosia, D. and Prins, R. "The effect of glycol on phosphate-doped CoMo/Al2O3 hydrotreating catalysts", *Journal of Catalysis*, **229**(2), pp. 424-438 (2005).

36. Matralis, H., Papadopoulou, C., and Lycourghiotis, A. "Fluorinated hydrotreatment catalysts effect of the deposition order of F-ions on F-CoMo/γ-AL2O3 catalysts", *Applied Catalysis A: General*, **116**(1-2), pp. 221-236 (1994).

37. Nava, R., Pawelec, B., Morales, J., Ortega, R.A., and Fierro, J.L.G. "Comparison of the morphology and reactivity in HDS of CoMo/HMS, CoMo/P/HMS and CoMo/SBA-15 catalysts", *Microporous and Mesoporous Materials*, **118**(1-3), pp. 189-201 (2009).

38. Gajardo, P., Grange, P., and Delmon, B. "Physicochemical characterization of the interaction between cobalt molybdenum oxide and silicon dioxide. 1. Influence of the cobalt-molybdenum ratio", *The Journal of Physical Chemistry*, **83**(13), pp. 1771-1779 (1979).

39. Ali, S.A., Ahmed, S., Ahmed, K.W., and Al-Saleh, M.A. "Simultaneous hydrodesulfurization of dibenzothiophene and substituted dibenzothiophenes over phosphorus modified CoMo/Al2O3 catalysts", *Fuel Processing Technology*, **98**, pp. 39-44 (2012).

40. Nava, R., Infantes-Molina, A., Castaño, P., Guil-López, R., and Pawelec, B. "Inhibition of CoMo/HMS catalyst deactivation in the HDS of 4,6-DMDBT by support modification with phosphate", *Fuel*, **90**(8), pp. 2726-2737 (2011).

41. Wang, Z., Fu, J., Deng, Y., Duan, A., Zhao, Z., Jiang, G., Liu, J., Wei, Y., and Zhao, S. "Synthesis of aluminum-modified 3D mesoporous TUD-1 materials and their hydrotreating performance of FCC diesel", *RSC Advances*, **5**(7), pp. 5221-5230 (2015).

42. Kanjanasoontorn, N., Permsirivanich, T., Numpilai, T., Witoon, T., Chanlek, N., Niamlaem, M., Warakulwit, C., and Limtrakul, J. "Structure-activity relationships of hierarchical meso-macroporous alumina supported copper catalysts for CO_2 hydrogenation: Effects of calcination temperature of alumina support", *Catalysis Letters*, **146**(10), pp. 1943-1955 (2016).

43. Faungnawakij, K., Tanaka, Y., Shimoda, N., Fukunaga, T., Kikuchi, R., and Eguchi, K. "Hydrogen production from dimethyl ether steam reforming over composite catalysts of copper ferrite spinel and alumina", *Applied Catalysis B: Environmental*, **74**(1), pp. 144-151 (2007).

44. Pazé, C., Gubitosa, G., Giacone, S.O., Spoto, G., Llabrés i Xamena, F.X., and Zecchina, A. "An XRD, FTIR and TPD investigation of NO2 surface adsorption sites of δ, γ Al2O3 and barium supported δ, γ Al2O3", *Topics in Catalysis*, **30**(1), pp. 169-175 (2004).

45. Wang, A., Wang, Y., Kabe, T., Chen, Y., Ishihara, A., and Qian, W. "Hydrodesulfurization of dibenzothiophene over siliceous MCM-41-supported catalysts", *Journal of Catalysis*, **199**(1), pp. 19-29 (2001).

46. Rodriguez, J.A., Chaturvedi, S., Hanson, J.C., and Brito, J.L. "Reaction of H2 and H2S with CoMoO4 and NiMoO4: TPR, XANES, time-resolved XRD, and molecular-orbital studies", *The Journal of Physical Chemistry B*, **103**(5), pp. 770-781 (1999).

47. Li, X., Chai, Y., Liu, B., Liu, H., Li, J., Zhao, R., and Liu, C. "Hydrodesulfurization of 4,6-dimethyldibenzothiophene over CoMo catalysts supported on γ-alumina with different morphology", *Industrial & Engineering Chemistry Research*, **53**(23), pp. 9665-9673 (2014).

48. Boufaden, N., Akkari, R., Pawelec, B., Fierro, J.L.G., Zina, M.S., and Ghorbel, A. "Dehydrogenation of methylcyclohexane to toluene over partially reduced silica-supported Pt-Mo catalysts", *Journal of Molecular Catalysis A: Chemical*, **420** (Supplement C), pp. 96-106 (2016).

49. Boufaden, N., Akkari, R., Pawelec, B., Fierro, J.L.G., Said Zina, M., and Ghorbel, A. "Dehydrogenation of methylcyclohexane to toluene over partially reduced Mo-SiO_2 catalysts", *Applied Catalysis A: General*, **502** (Supplement C), pp. 329-339 (2015).

Biographies

Mansoureh Zarezadeh-Mehrizi received her BSc degree in Pure Chemistry from Alzahra University in 2006. She obtained her MSc and PhD degrees in Inorganic Chemistry from University of Tehran in 2009 and 2014, respectively, under the supervision of Dr. Alireza Badiei. Her research interests include porous materials and catalysis.

Ali Afshar Ebrahimi is a PhD Student in Chemical Engineering. He received his BSc, MSc, and PhD from Amirkabir University of Technology. He is an Assistant Professor in IPPI, and his research studies are focused on hydrotreating and catalytic cracking of heavy petroleum cuts.

Azam Rahimi is currently a Professor at the Department of Polymer Science, Iran Polymer and Petrochemical Institute. She obtained her PhD degree from Michigan State University. She has about 40 years of scientific editing, teaching, and research experience. Her research interests include synthesis of inorganic compounds, drug delivery systems, and nanocomposites.